# Effect of Side-Walls on Flapping-Wing Power-Generation: an Experimental Study

F. Karakas and I. Fenercioglu†

*Istanbul Technical University, Department of Astronautical Engineering, Istanbul, 34469, Turkey*

†*Corresponding Author Email: fenercio@itu.edu.tr*

## ABSTRACT

Effect of constrained flow is investigated experimentally for a flapping foil power-generator. The flow structures around and in the near wake of a flat plate placed between two side walls are captured via PIV technique with simultaneous direct force measurements in uniform flow at Re = 10 000. The rectangular flat plate oscillates with periodic non-sinusoidal pitching and plunging motions about its 0.44 chord position with stroke reversal times ($\Delta T_R$) of 0.1 (rapid reversal) to 0.5 (sinusoidal reversal), phase angles of $\phi = 90°$ and $110°$, plunge amplitude of 1.05 chords and pitch amplitude of $73°$ at a constant reduced frequency of $k = 0.8$. The non-dimensional distances between the side walls and the oscillating flat plate are $d_w = 0.1$, 0.5 and 1.0. Airfoil rotation speed dictates the strength, evolution and timing of shedding of leading and trailing edge vortices; as the stroke reversal time is decreased, earlier shedding of stronger vortices are observed. Increasing the phase angle between the pitching and plunging motions decreases the power generation efficiency for all cases. The highest power extraction coefficient is acquired for the non-sinusoidal case of $\Delta T_R = 0.4$ in free flow. Optimum choice of side-wall distance improves power generation of flapping foils compared to free flow performance, up to 6.52% increase in efficiency is observed for the non-sinusoidal case $\Delta T_R = 0.4$ with $d_w = 0.5$, with remarkable enhancements for the sinusoidal case; 27.85% increase is observed with $d_w = 0.5$ and 43.50% increase with $d_w = 1.0$ where both cases outperform the highest power generation efficiency of the finite flat plate with non-sinusoidal flapping motion.

Keywords: Constrained flow; Oscillating foil; Flapping wing; Power generation; PIV.

## NOMENCLATURE

| | | | |
|---|---|---|---|
| $c$ | chord length | $P$ | power developed |
| $C_p$ | power coefficient | $\bar{P}$ | time-averaged power |
| $\bar{C}_P$ | time-averaged power coefficient | $P_a$ | maximum power available |
| $C_{P\,total}$ | total power coefficient | $Re$ | Reynolds number based on free stream velocity and foil chord |
| $C_{Py}$ | power coefficient due to plunging motion | | |
| $C_{P\theta}$ | power coefficient due to pitching motion | $s$ | span length |
| $d$ | maximum total transverse distance swept by the foil trailing edge | $St$ | Strouhal number |
| | | $t$ | time |
| $d_w$ | minimum distance between the trailing edge and the side wall inserts non-dimensionalized by $c$ | $T$ | period of oscillation |
| | | $U_\infty$ | free-stream velocity |
| | | $V_y$ | translational velocity |
| $f$ | flapping frequency | | |
| $h$ | non-dimensional plunge amplitude to chord ratio | $\Delta T_R$ | stroke reversal time, as a fraction of the flapping period |
| $hc$ | plunge motion amplitude | $\eta$ | efficiency of power extraction |
| $h_w$ | distance between the two side wall inserts non-dimensionalized by $c$ | $\theta$ | pitch motion velocity |
| | | $\theta_o$ | pitch motion amplitude |
| $k$ | reduced frequency | $\phi$ | phase angle between pitching and plunging motions |
| $L$ | transverse force on the foil | | |
| $M$ | moment about the foil pivot point | | |

## 1. INTRODUCTION

Some of the many possible ways to exploit clean and sustainable energy is by wider use of wind and water resources. Power can be extracted from the flowing fluids in different ways. Traditional power generation via surrounding fluids mainly depends on turbines. However, turbines met criticism because of their huge mass, danger to wildlife and requirement of minimum flow velocity to be financially feasible (Westwood 2004). The use of flapping wings was proposed to be an alternative to conventional power generators and the feasibility of energy extraction from the flow by a harmonically oscillating wing was experimentally proved by McKinney and Delaurier (1981) with comparable efficiency to that of a rotational windmill.

Leading edge vortex (LEV) generation and shedding plays a significant role in power generation (Young *et al.* 2014). The timing of LEV shedding is particularly critical in maximizing the power extraction efficiency via varying the local surface pressure distribution (Kinsey and Dumas 2008; Zhu and Peng 2009). The LEV is also recognized in biomimicking studies as core to lift generation during hover and forward flight (Shyy *et al.* 2010). For a purely plunging foil, generation of thrust is achieved by the strong leading edge suction. Due to the pressure gradients associated with high flow velocities, the flow can no longer remain attached and separation occurs forming the LEV. The inherent rotation of the fluid in the LEV leads to low pressures at the core of the vortex and this low pressure region results in an enhancement of the force normal to the oncoming flow. In power generation applications, it is desired to have the lift force aligned with the direction of the foil's plunging motion. It is also essential for a power generator to have an angle of attack large enough to create flow separation and LEV formation to assist instantaneous enhancement of lift.

Most investigations on oscillating wing power generators are based on sinusoidal pitching and/or plunging motions, which are the most fundamental harmonic profiles for flapping motions (Naderi *et al.*, 2016). However, in nature, the high propulsion efficiency of flying and swimming animals can be achieved by non-sinusoidal locomotion trajectories (Licht *et al.* 2010). Inspired by this biomimicking mechanism, non-sinusoidal oscillatory motions draw considerable attention in recent studies (Jones and Platzer 2010; Platzer *et al.* 2014; Xiao *et al.* 2012). Platzer *et al.* (2010) and Ashraf *et al.* (2011) numerically investigated non-sinusoidal motion of an oscillating-wing power generator with different pitch stroke reversal times and achieved up to 17% increase in power generation and up to 15% increase in efficiency for non-sinusoidal flapping compared to those of sinusoidal motions. Increase in both power generation and efficiency were also observed for a flapping foil power generator using the same motion parameters (Fenercioglu *et al.* 2015) and good agreement was found between experimental results and 2D Navier-Stokes simulations. Their results showed the beneficial aspects on efficiency enhancement from non-sinusoidal motion profile.

In order to achieve sufficient power output using flapping foil power generators, the plunge amplitude needs to be comparable to the chord length; it was shown by Dumas and Kinsey (2006) that the power coefficient linearly increases with increasing plunge amplitude. However, the efficiency does not always follow the same trend; Kinsey and Dumas (2008) pointed out for a flapping wing power generator that 90° is the optimum phase angle between the pitching and the plunging motions for maximum energy extraction. The pivot location has a similar effect as changing the phase angle between pitch and plunge; when the pivot point is just in front of the mid-chord position, the efficiency of power generation takes a maximum value (Davids 1999). A previous study (Fenercioglu *et al.* 2015) also showed improvement in performance when the pitch pivot location was changed from quarter point location to mid-chord. In another study (Ashraf *et al.* 2009), it was indicated that highest performance can be achieved for 0.44-0.46 chord pivot location and optimum power generation was acquired when the pivot location was positioned between 0.33 to 0.5 chords from the leading edge (Peng and Zhu 2009).

The majority of experimental and numerical investigations in the literature focuses primarily on two-dimensional wing geometries in free stream and provides a great deal of insight into the formation and transition of the LEV. However, in real-life applications, the end effects due to finite-length wingspan and solid side walls will have an effect on the performance of the oscillating-wing power-generator. Three dimensionality effects of the non-sinusoidally flapping flat plate power generator was previously investigated experimentally in free stream and overall efficiency reduction for all tested cases were observed due to the tip vortex interactions with the LEV and the near wake of the flat plate (Karakas and Fenercioglu 2015). Another concern to take into account in the design of a flapping foil power generator is the interactions with neighboring foils in energy harvesting farms and the interactions when the flapping foil is placed under sailing ships as proposed by Platzer *et al.* (2014). When a flapping foil is positioned in close proximity to solid walls, the ground effect may affect the performance of the power generator. Ground effect increases the pressure on the lower surface of the foil when the distance between the foil and the wall is below a critical value. Wu (2013) concluded from his numerical simulation that high frequency and small distance are helpful for generation of thrust force and large lift force. Wu (2014) also indicates that the net power extraction efficiency is improved due to the ground effect. However, experimental research of the ground effect to evaluate the performance of a flapping foil power generator is limited in the literature. Therefore, investigation on the effects of solid side-walls in three dimensional free and constrained flows needs to be conducted in order to fully understand the physics of the flow around and in the near wake of oscillating wings.

In this study, an experimental investigation was performed to aid the design and development of a catamaran-type sailing ship based renewable power generator with underwater operating flapping-wings. The hull was modeled as side-walls in each side of a finite flat plate flapping with non-sinusoidal periodic pitch and combined plunge motions. The effect of side-wall distances from the flapping flat plate, pitch stroke reversal rates and variations in phase angle between the pitching and plunging motions are investigated via detailed quantitative evaluation of flow structures and simultaneous direct force measurements with the objective to provide further insight into the optimum operation parameters of a potential flapping foil power generator.

## 2. EXPERIMENTAL SETUP

The experiments are performed in the closed-circuit, large scale water channel located in the Trisonic Laboratories at the Faculty of Aeronautics and Astronautics of Istanbul Technical University. It has a main test section of 790 mm depth and 1010 mm width. Detailed description of the flow facility can be found in Fenercioglu and Cetiner (2012, 2014), Son and Cetiner (2016). A non-profiled flat plate with rectangular cross section is used in this study considering low manufacturing costs and power extraction enhancement results as demonstrated by Usoh *et. al.* (2012). The transparent Plexiglas flat plate with chord length of $c = 10$ cm and span of $s = 30$ cm is mounted in a vertical cantilevered arrangement in the water channel. Considering the abovementioned studies (Platzer *et al.* 2014; Ashraf *et al.* 2009), the pitch pivot location is positioned at 0.44 chord distance from the leading edge. The rectangular flat plate model is connected to a servo motor which provides the pitching motion via a coupling system which itself is connected to a linear table which provides the plunging motion. An end plate with 30° outward bevel is suspended from the top of the channel to eliminate free surface effects. This study considers the oscillating-foil power generator close to its proposed operating conditions; i.e. fully submerged finite flapping wing with an upper end plate which represents the symmetry plane as customary in the literature (Jones *et al.* 2011; Visbal *et al.* 2013; Son and Cetiner 2015).

The digital particle imaging velocimetry (PIV) system with Dynamic Studio software (Dantec Dynamics A/S) is used to record the quantitative evolution of flow structures around and in the near wake of the flat plate. The flow is illuminated by a dual cavity Nd:Yag laser (max. 120 mJ/pulse) oriented horizontally at the flat plate's mid-span plane. The water is seeded with silver coated glass spheres of 10μm mean diameter. Two 10-bit cameras with 1600×1200 pixels resolution are positioned underneath the water channel and the two double-frame images from the two cameras were stitched before interrogation with an in-house code using two marker points to allow for a larger field of view in the illumination plane. Three dimensionality effects were investigated by recording the flow structures along the span of the flat plate at three different

illumination planes of half-span (1/2 span), quarter span (1/4 span) and 2mm above the tip. PIV image acquisition to investigate the effect of side-walls on power generation was performed at mid-span illumination plane. The experimental arrangement with side-walls is shown in Fig. 1.

400 instantaneous images were acquired for 25 cycles of motion for each experimental data set and phase averaged so that one period of the airfoil motion is represented with 16 images. The acquired PIV images were interrogated using a double frame, cross-correlation technique with a window size of 64×64 pixels and 50% overlapping in each direction. The final grid resolution of velocity vectors is 5.8 mm × 5.8 mm in the plane of the flow which corresponds to a resolution of $0.058c \times 0.058c$. The resulting measurement plane is represented with approximately 3400 velocity vectors. The total velocity uncertainty in the PIV experiments is less than 2%.
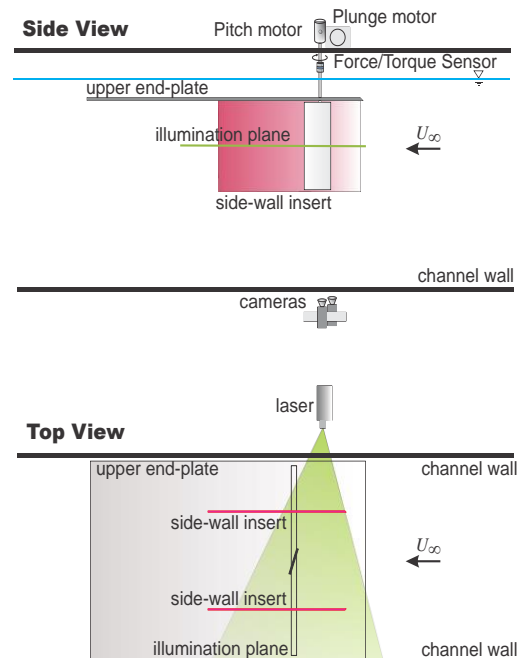


**Fig. 1. Top and bottom views of experimental setup.**

The forces and moments acting on the flapping foil were measured using a six-component ATI Nano17 IP68 Force/Torque sensor (ATI Industrial Automation, Inc.). The sensor was attached to the vertical cantilevered arrangement between the flat plate model and the pitch servo motor, oriented with its cylindrical *z*-axis normal to the pitch-plunge plane. Dynamic force and moment data was collected for 30 periods with a sampling rate of 10 000 Hz. The data was block averaged within a window of 100 data points which resulted in an effective 100 Hz sampling rate and then phase averaged to downscale data to one period. A parabolic low pass FFT filter was applied to reduce the high frequency noise and to omit the effect of natural frequency of the system. Since the Force/Torque sensor rotates with the model undergoing pitching and plunging motions, the lift

force was computed by transforming the measured forces dynamically for the motion kinematics for each test case, following the calculations given by Fenercioglu *et al.* (2015).

The non-dimensional instantaneous power coefficient $C_P$ is defined as:

$$C_p = \frac{P}{0.5\rho U_\infty^3 sc} \tag{1}$$

and $P$ is the developed power:

$$P = LVy + M\theta \tag{2}$$

where the transverse force on the foil is $L$, translational velocity is given with $V_y$, the moment about the foil pivot point is $M$ and the pitch motion velocity is $\theta$.

The total power coefficient $C_{P\ total}$ is the sum of power coefficient due to plunging motion $C_{Py}$ and power coefficient due to pitching motion $C_{P\theta}$:

$$C_{P\ total} = C_{Py} + C_{P\theta} \tag{3}$$

$$C_{Py} = LV_y / 0.5\rho U_\infty^3\ sc \tag{4}$$

$$C_{P\theta} = M\theta / 0.5\rho U_\infty^3\ sc \tag{5}$$

Efficiency of power extracted, where $d$ is the maximum total transverse distance swept by the foil trailing edge, is given as:

$$\eta = \bar{C}_P\ c/d \tag{6}$$

where $\bar{C}_P$ is the mean power coefficient.

The pitch and plunge motions of the flat plate test model were accomplished with Kollmorgen/Danaher Motion AKM33E and AKM54K servo motors respectively. The servo motors were connected to a computer via Servo STAR S300 digital servo amplifiers for pitching motions and Servo STAR S700 for plunging motions, and motor motion profiles were generated by a signal generator Labview VI (Virtual Instrument) for the given amplitude and frequency. The same VI triggered the PIV system and synchronization was achieved using a National Instruments PCI-6601 timer device.

Kaya and Tuncer (2007) emphasized that the thrust and/or propulsive efficiency are optimized by using non-sinusoidal pitching and plunging motions. For maximum thrust generation, they showed that the flapping airfoil should stay at about a constant angle of attack during the upstroke and the downstroke motions and reverse direction at the minimum and maximum plunge positions. Platzer *et al.* (2009) characterized the motion kinematics of a flapping-wing power generator by a variable of reversal times as a fraction of the total cycle $\Delta T_R$, ranging from $\Delta T_R = 0.1$ for rapid reversal to $\Delta T_R = 0.5$ for purely sinusoidal motion. The variation of periodic motion of the flat plate is given in Fig. 2, with a period of constant translational velocity combined with a constant pitch angle, followed by a reversal of direction and pitch angle.
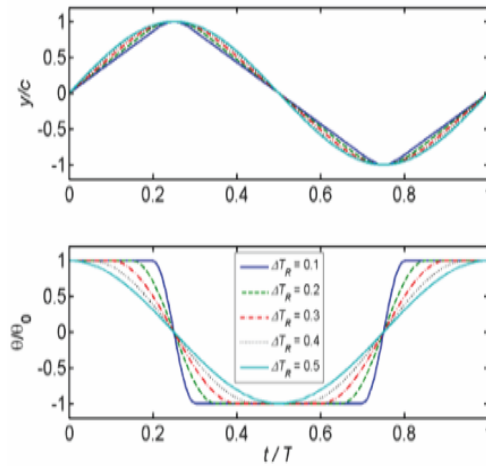


**Fig. 2. Variation of plunge and pitch motions (Plazter *et al.* 2009).**

Here $y$ (t) represents the plunging motion and $\theta$(t) is the pitching motion. In this study, the plunge motion amplitude of the flat plate is $h = 1.05$ non-dimensionalized by chord and the pitch motion amplitude is $\theta_0 = 73°$, as consistent with previous studies on an oscillating-wing power-generator (Ashraf *et al.* 2011; Fenercioglu *et al.* 2015).

The reduced frequency ($k$) is defined as:

$$k = \frac{2\pi f c}{U_\infty} \tag{7}$$

and set constant at $k = 0.8$ throughout this study. The free stream velocity of the water channel is $U_\infty = 0.1$ m/s corresponding to Reynolds number of Re = 10 000. The flat plate profile undergoes combined non-sinusoidal pitching and plunging oscillations with equal flapping frequencies of $f = 0.125$ Hz. The investigated cases consider the phase differences of $\phi = 90°$ and $110°$, where pitch leads the plunge motion.

In order to investigate the effect of side walls, two transparent Plexiglas plates with $5c$ length, $0.05c$ thickness and $30°$ outward bevel are suspended from the top of the water channel on both sides of the flapping flat plate. The distance between the side walls and the oscillating flat plate ($d_w$) is set such that the minimum non-dimensional distance between the walls and the flat plate at its minimum and maximum positions for the case of $\Delta T_R = 0.1$ and $\phi = 110°$ is $d_w = 0.1$, 0.5 and 1.0, non-dimensionalized by chord length. After the side-walls are positioned for the rapid reversal case, data acquisition was carried on for all $\Delta T_R$ and phase angle cases before moving the side-walls to the next position.

## 3. RESULTS

The vorticity concentrations around and in the near wake of the finite flat plate undergoing non-sinusoidal flapping with rapid stroke reversal time ($\Delta T_R = 0.1$) with phase angle between the pitching and plunging motions is $\phi = 90°$ in free flow is given in Fig. 3. The vortical structures are shown at

the three laser illumination planes along the span. During the experiments, 16 images were acquired for one period of the flat plate for a total of 25 periods of oscillatory motion. The flow is from left to right in the figures. Since the flapping motion of the flat plate is symmetrical, the formation and shedding of positive and negative vortices are also symmetrical throughout the motion cycle; thus half period of flat plate's motion from the start-up position is given herein. The first image in each figure shows the flat plate at its mid-plunge position where it starts its motion with high angle of attack of $\theta_0 = 73°$ ($t = 0$). The flat plate first moves upward, the first image in the second row ($t = 4T/16$) corresponds to the flat plate's maximum plunge position where it continues its downward motion after rapid non-sinusoidal reversal ($\Delta T_R = 0.1$) of direction and pitch angle, and the last image shows the test model approaching its mid-plunge position as its downstroke motion continues. In order to perform a direct comparison of all cases, the vorticity contour levels are set constant to minimum non-dimensionalized vorticity level of $[\omega c/U_\infty]_{min} = \pm 0.0025$ and incremental non-dimensionalized vorticity level of $\Delta[\omega c/U_\infty] = 0.0025$ for all cases.

Inspecting the PIV results at 1/2 span laser illumination plane, the negative vortex formation from the leading edge on the upper surface can be noticed at flat plate's mid-plunge position during upstroke ($t = 0$). The roll-up radius of this clockwise rotating vortex grows as the flat plate continues the upstroke motion while a positive vortex starts to form from the trailing edge. After flat plate reaches its maximum plunge amplitude position and changes direction to continue its downstroke motion, the negative and positive vortices are eventually shed into the wake ($t = 6T/16$). This process is reversed during downstroke motion, where the positive vortex rotating counterclockwise forms on the flat plate's lower surface and is shed after pitch reversal. It can be seen from the 1/4 span and tip planes in Fig. 3 that the clockwise rotating vorticity formation on the upper surface of the flat plate experiences a pull-down effect along the span. This negative vortex stays closer to the upper surface at the quarter-span illumination plane and stretches out at the tip of the model. The formation trend of flow structures along the span is alike for all the sinusoidal and non-sinusoidal pitch reversal cases investigated in this study; the negative LEV tend to shrink and stays closer to the upper surface of the flat plate at the 1/4-span plane. The vortical structures move along the span towards the tip where they stretch out into the wake and lift off the surface at the tip plane rather than detach and dissipate ($t = 2T/16$). Similar vortex formations were identified by Kruyt *et al.* (2015) where an attached LEV along the upper surface of their finite model smeared-out and detached outboard at high angle of attack values and by Jones *et al.* (2011) where they reported that the shed vortices tend to lift off the wing surface near the wing tip, but remain close to the surface further inboard.
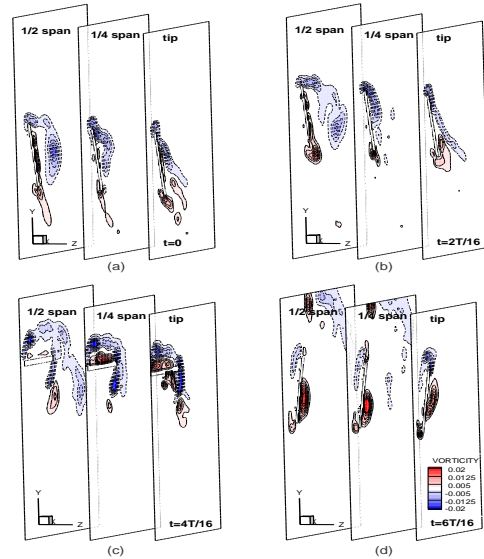


**Fig. 3. Vorticity patterns at three laser planes along the span of the flat plate for $\Delta T_R = 0.1$, $\phi = 90°$.**

The mean power coefficient values obtained by direct force measurements are given in Fig. 4 for all test cases. It can be noticed that none of the rapid pitch reversal cases ($\Delta T_R = 0.1$) can attain a positive mean power coefficient regardless of free or constrained flow. Fig. 4 also shows that increasing the phase angle between the pitching and plunging motions from $\phi = 90°$ to $\phi = 110°$ results in lower mean power production for all cases, again consistent with the previous study (Fenercioglu *et al.* 2015). Since the pitching motion leads the plunging motion, the flat plate begins its pitch reversal earlier when the phase angle between the pitching and plunging motions is increased from $\phi = 90°$ to $110°$, which in turn results in earlier detachment and shedding of the vortices from the leading edge with the consequence of lower power production. Delaying the LEV detachment throughout the flapping cycle is essential to high power generation (Kinsey and Dumas, 2008) and a jet-like reverse Karman vortex street indicates thrust generation of an oscillating airfoil (Jones *et al.* 1998).
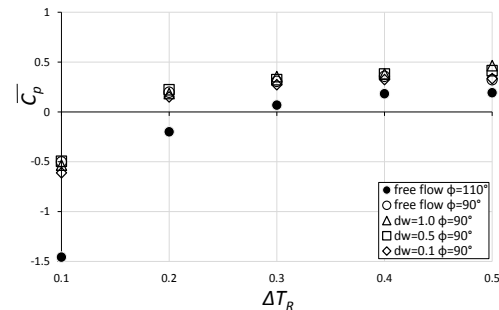


**Fig. 4. Mean power coefficients for all cases.**

400 instantaneous images acquired by the PIV system are averaged to examine the effect of phase angle on the time averaged vorticity and free stream value subtracted time-averaged velocity patterns for the non-sinusoidal case with pitch stroke reversal

time of $\Delta T_R = 0.2$ in free flow. Minimum non-dimensionalized vorticity level of $[\omega c/U_\infty]_{min} = \pm 0.00025$ and incremental non-dimensionalized vorticity level of $\Delta[\omega c/U_\infty] = 0.00025$ are used for time-averaged vorticity contour levels. It can be seen from Fig. 4 that the $\phi = 90°$ case gives positive power production while the flat plate with $\phi = 110°$ case gives negative mean power coefficient over one period of its oscillation cycle. The time-averaged wake-flow is visible in Fig. 5a where the clockwise rotating negative vortex stays on the upper row and the counter clockwise rotating positive vortex stays on the lower low. Although it is only possible to observe approximately $1.5c$ of the wake behind the flat plate, an inner jet formation is visible inside the wake flow for the $\phi = 110°$ case (Fig. 5b). The vortex pair is formed by a negative vortex on the upper row and a positive vortex on the lower low with a smaller branch of positive vortex on the upper row and a negative vortex on the lower row forming a jet-like flow inside the outer branches of the enclosing wake-flow and crisscrossing each other at around one chord distance downstream of the flat plate's trailing edge to form an inner wake. Similar bifurcation of wake flow was also observed in Hu *et al.*'s (2011) experimental study and in their subsequent numerical study (Yu *et al.* 2013). As also given in Fenercioglu *et al.* (2015) for a 2D flapping airfoil profile, the power production capacity of the oscillating airfoil is strongly affected by such "inner" vortices with unfavorable induction effect on the wake. When the phase angle is changed from $\phi = 90°$ to $\phi = 110°$, there is a significant decrease in efficiency to over 30.52%.
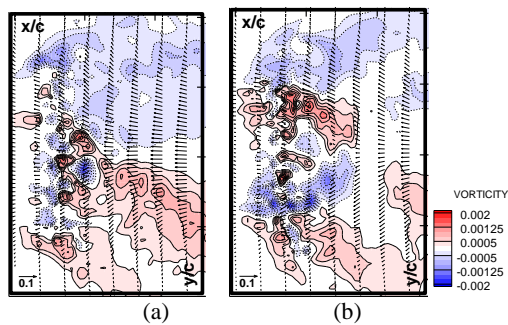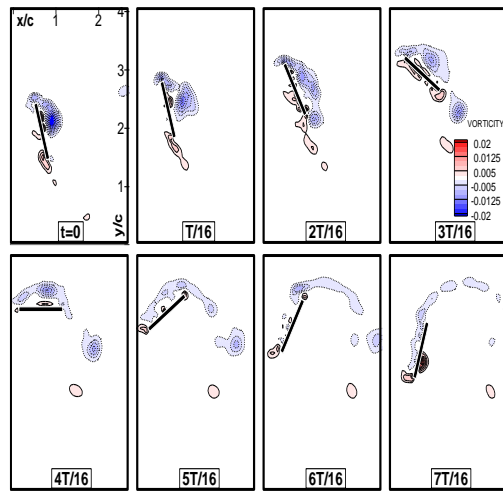


**Fig. 5. Time-averaged velocity and vorticity patterns for $\Delta T_R = 0.2$ in free flow a) $\phi = 90°$, b) $\phi = 110°$.**

For the non-sinusoidal pitch reversal cases in free flow, as $\Delta T_R$ is increased from $\Delta T_R = 0.1$ to $\Delta T_R = 0.4$ so that the airfoil's rotation speed during reversals is decreased from square-like form to near-sinusoidal, the formation of negative and positive vortices from the leading and trailing edges also slows down and shedding into the wake occurs with lower strength. The acceleration and deceleration of the flat plate results in higher added mass during pitch stroke reversals (Turam *et al.* 2015) which in turn lower the power consumption and increases the power production. This phenomenon can be observed in Figure 6a where the instantaneous vorticity patterns are given for half motion cycle of the flat plate with
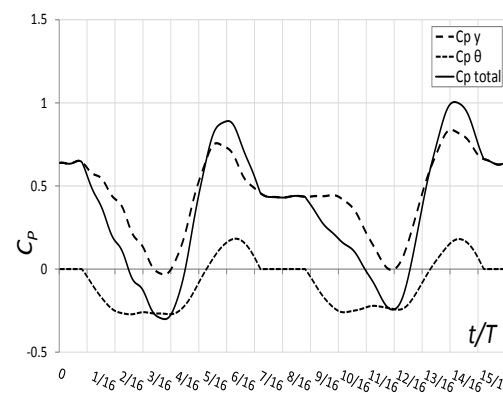
pitch reversal rate of $\Delta T_R = 0.4$ in free flow along with the instantaneous total power coefficients due to pitching ($C_{P\theta}$) and due to plunging ($C_{Py}$) over one period of motion (Fig. 6b). In Figure 6a, half period of the oscillatory motion of the flat plate is represented with 8 images and the laser illumination plane is at 1/2 span position. In line with the results from a previous study (Fenercioglu *et al.* 2015) where 2D experiments and numerical simulations were performed, the performances of non-sinusoidal cases are superior to sinusoidal pitch reversal. It is conspicuous that the stroke reversals have major effect on the time averaged total power coefficient and the timing of the formation and shedding. The interaction of the LEV with the flat plate dictates the time averaged power output; the contribution of plunging motion to the total power coefficient can be sustained during the translation phase of the flat plate. As can be seen in Figure 6b, the power coefficient sustains its value when the pitch angle is constant, between $t = 15T/16 - T/16$ during upstroke and $t = 7T/16 - 9T/16$ during downstroke (Fig. 6a). The optimal propulsive efficiency of $\eta = 17.19\%$ and the maximum mean power coefficient of $\bar{C}_P = 0.36$ are obtained for the finite flat plate with non-sinusoidal pitch stroke reversal of $\Delta T_R = 0.4$ and phase angle of $\phi = 90°$ in free flow

The effect of wall proximity on power production is investigated for the finite flat plate flapping with phase angle of $\phi = 90°$. The mean power coefficients for all cases in Fig. 4 show that constrained flow with the non-dimensional wall distance of $d_w = 0.5$ and $1.0$ increase the overall performance of power generation for all cases, however this enhancement is not adequate to increase the rapid pitch reversal case's ($\Delta T_R = 0.1$) mean power coefficient to positive range. The improvement in total power coefficient in sinusoidal pitch reversal case is particularly remarkable; 43.50% increase is achieved compared to the free flow case when the non-dimensional side-wall distance is set to $d_w = 1.0$ and 27.85% increase is achieved when $d_w = 0.5$. On the other hand, it can be noticed in Fig. 4 that very close proximity of the side-walls ($d_w = 0.1$) have most unfavorable effect on flapping foil power generation for all test cases.

The best performance for the non-sinusoidal motion in constrained flow is also achieved for the $\Delta T_R = 0.4$ case, however when the side walls are spaced at $d_w = 0.5$, the sinusoidal case outperforms the non-sinusoidal case by 8.85%. In their numerical study using a sinusoidally flapping airfoil, Wu *et al.* (2104) defines an elongated high pressure region on the upper surface of the airfoil as it gets closer to an upper wall causing a negative lift force that they attribute to the shear-induced effect (Saffman, 1965). The flat plate also experiences higher added mass as the pitch reversal rate is increased by decreasing $\Delta T_R$ and this high added mass possibly increases the power consumption and lowers the power production as also pointed out by Karakas *et al.* (2016), which might result in sinusoidal cases to perform better than non-sinusoidal cases in constrained flow.

(a)



(b)

**Fig. 6. $\Delta T_R = 0.4$, $\phi = 90°$, free flow a) Vorticity patterns, b) Instantaneous power coefficients.**

Figure 7 shows the vorticity patterns around and in the near wake of the sinusoidally oscillating flat plate in free and constrained flow. Figs. 8a and 8b show the time histories of the contributions of the plunging and pitching motions to the total power coefficient respectively for the same case. The vorticity patterns show that a negative vortex forms after the pitch reversal and continues its growth as the flat plate maintains the upstroke motion. After sinusoidal reversal of direction and pitch angle, this negative LEV detaches and dissipates into the wake, resulting in a decrease in the instantaneous power coefficient due to plunging motion ($C_{Py}$). As the side-walls get closer to the flapping flat plate, the negative vortex covering the upper surface re-attaches towards the trailing edge of the flat plate during its upstroke motion ($t = 2T/16$). Although minor, this interaction with the wall results in a small increase in the instantaneous power coefficient due to pitching motion ($C_{P\theta}$) when the non-dimensional side-wall distance is $d_w = 0.1$, slightly compensating for the loss in power production during stroke reversals, though the decrease in $C_{Py}$ is much higher. When the flat plate is flapping close to the side-walls as in the cases with $d_w = 0.5$ and $d_w = 0.1$, it can be noticed that the clockwise rotating negative vortex is flatter than that of the

free stream case (Figure 7c and Figure 7d), the side-wall compresses the vortices causing them to stay attached to the upper surface of the flat plate. After pitch stroke reversal, the detachment is delayed when the side-walls are positioned close to the flapping flat plate and the negative vortex is formed of small localized cells, stretching out into the wake. This brief interaction with the side-walls results in an increase in the instantaneous power coefficient for $d_w = 0.5$ and $d_w = 1.0$ cases ($t = 6T/16$) followed by a small decrease at $t = 6T/16$ - 7T/16 where the flattened shed vortex sweeps the side wall before dissipating into the wake. This loss is quickly recovered when $d_w = 0.5$ and $d_w = 1.0$, where the constrained flow show marked improvements on power production for the sinusoidal case throughout the plunging motion as compared to free flow ($t = 7T/16$ - 9T/16). Since the flat plate and the kinematic motion are symmetrical, the same process holds during the downstroke motion with same effect of side walls; notable increase in power coefficient is observed after pitch stroke reversal when the flat plate approaches the side-wall at the minimum plunge position during its downstroke motion ($t = 9T/16$ - 10T/16). The mean power coefficient value for the sinusoidal pitch reversal case is significantly increased by 43.50% compared to the free flow case when the non-dimensional side-wall distance is set to $d_w = 1.0$ and by 27.85% when $d_w = 0.5$.

In Fig. 7d where the vorticity plots are given where the side-walls are set closest ($d_w = 0.1$) to the sinusoidal flapping flat plate, it can be noticed that as the flat plate completes its pitch rotation at the end of its upstroke motion and begins its downstroke motion, a weak positive vortex forms on the surface of the upper side-wall and interacts with the negative vortex detached from the upper surface of the flat plate from its trailing edge at $t = 6T/16$. Such additional vortex caused by the presence of a side-wall was also noted by Rehimi *et al.* (2011) for a stationary cylinder placed between two walls. This positive vortex moves slower than the negative vortex, where we see it linger near the upper side-wall at $t = 7T/16$ while the negative vortex has left the observable flow field area. The instantaneous power coefficient due to plunging motion of this case in Fig. 8a shows the decrease at $t = 6T/16$ which can be associated with the formation of this counter clockwise rotating positive vortex generated on the wall.

Figure 9 shows the mean power coefficient values for the sinusoidal case in constrained and free flow with the three-dimensional and finite test models, where the free flow side-wall distance is denoted with $d_w = 4$ considering the water channel dimensions. The maximum mean power coefficient of $\bar{C}_P = 0.43$ is obtained in two dimensional cases for the finite flat plate with non-sinusoidal pitch stroke reversal of $\Delta T_R = 0.4$ and phase angle of $\phi = 90°$ in free flow (Karakas *et al.*, 2016). However, 17.02% decrease in mean power coefficient is observed when the same motion parameters are used in the three dimensional setup.
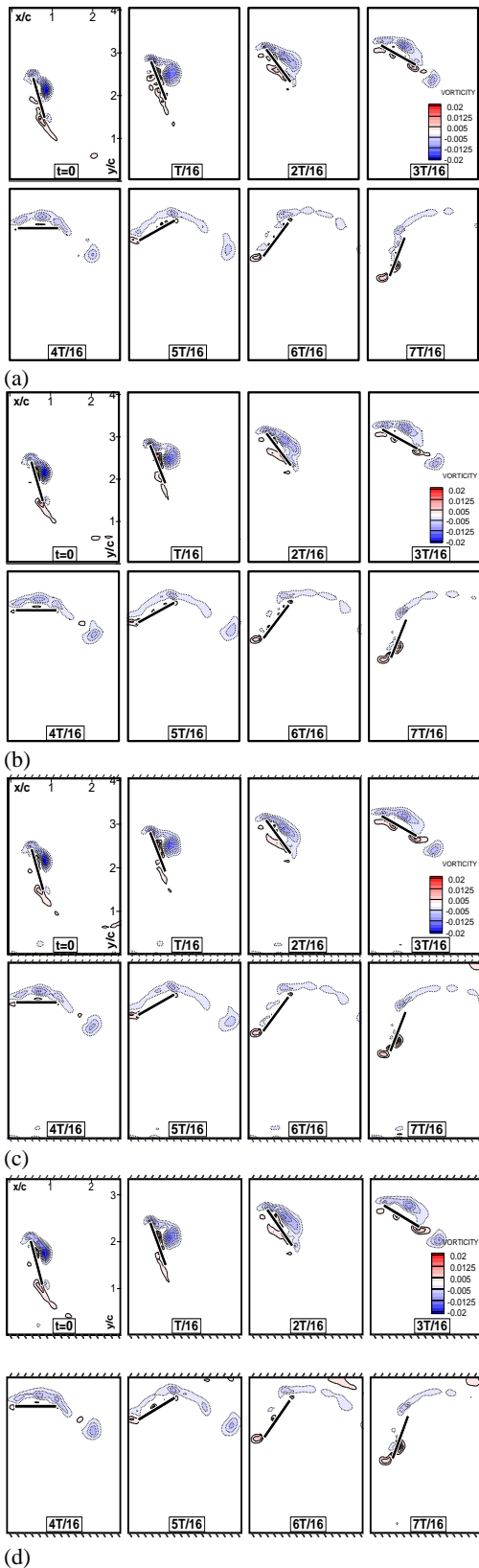
(a)



(b)



(c)



(d)

**Fig. 7. Vorticity patterns for sinusoidal cases ($\Delta T_R = 0.5$), $\phi = 90°$, a) free flow, b) $d_w = 1.0$, c) $d_w = 0.5$, d) $d_w = 0.1$.**

The mean power coefficient values show that constrained flow with the non-dimensional wall distance of $d_w = 0.5$ increases the overall

performance of power generation in both 2D and 3D cases. The side wall effect enhances the power output for the sinusoidal ($\Delta T_R = 0.5$) and near-sinusoidal ($\Delta T_R = 0.4$) cases. In a previous study for 2D flow (Karakas *et al.* 2016), it was observed that a 29.57% increase in efficiency can be achieved when the side walls are placed at $d_w = 0.5$ for the sinusoidal flapping flat plate as compared with the free flow. In this study for the 3D cases, a 27.86% increase in efficiency is achieved with the same side wall distance ($d_w = 0.5$) in sinusoidal case compared with the free flow. Moreover in 3D cases, all side wall distances examined in this study enhance the power extraction efficiency and the efficiency increases with the increasing side-wall distance. But there is a sudden decrease in efficiency and mean power coefficient when the side walls are removed to get free flow, which shows that there is an optimum side wall distance that gives the maximum power generation efficiency.
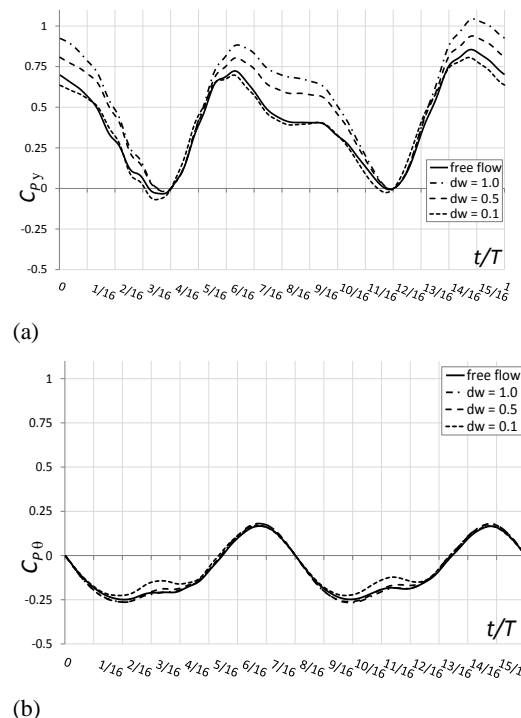


(a)



(b)

**Fig. 8. Instantaneous power coefficients for $\Delta T_R = 0.5$, $\phi = 90°$ a) due to plunge, b) due to pitch.**



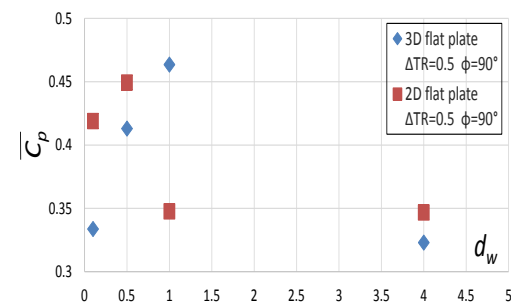**Fig. 9. Mean power coefficients for $\Delta T_R = 0.5$, $\phi = 90°$ for the three-dimensional cases and the two-dimensional cases.**

Although the two-dimensional cases perform better than their counter parts of three-dimensional test cases, real life applications will consider finite flapping foil power generators. The degradation in performance is due to LEV and tip vortex interactions in three- dimensional cases which create shrinkage in size in the vortical structures at the upper surface where they tend to stay closer to the flat plate. The separated tip vortex interferes with the wake of the flat plate and reduces the overall efficiency.

## 4. CONCLUSION

In this experimental study, effect of side-walls on power generation is examined for possible applications to catamaran-type sailing ship based flapping-wing renewable hydropower generators. The flow structures and the forces acting on a finite flat plate undergoing non-sinusoidal pitching and plunging motions in free and constrained flow are investigated via detailed quantitative flow visualization and simultaneous direct force measurements. Reynolds number of 10 000, non-dimensional plunge amplitude of $h = 1.05$, pitch amplitude of $\theta_o = 73°$ and phase angles of $\phi = 90°, 110°$ are considered in this study. The test model was chosen a flat plate with rectangular cross section and the pitch pivot was positioned at 0.44 chord location from the leading edge. The minimum distance between the trailing edge at the flat plate's minimum and maximum positions after pitch reversals and the side wall inserts was varied as $d_w = 0.1, 0.5$ and 1.0 chord lengths.

The vorticity concentrations around and in the near wake of the flapping flat plate show that early shedding of higher strength vortices occur when the pitch reversal rate is increased. Increasing the phase angle from $\phi = 90°$ to $110°$ also results in earlier shedding of the LEV due to earlier pitch reversal, with the consequence of lower power generation. LEV and tip vortex interactions are observed near the tip of the finite flat plate where vortical structures shrink in size and stretch out to the wake losing their strength to roll up. The highest mean power coefficient of $\bar{C}_P = 0.36$ and power extraction efficiency of $\eta = 17.19\%$ was observed for the non-sinusoidal case in free flow with pitch stroke reversal time of $\Delta T_R = 0.4$ and phase angle of $\phi = 90°$. None of the rapid pitch stroke reversal cases were able to extract power from the surrounding flow. The cases with negative mean power coefficient are associated with jet-like inner flow inside the main branches of surrounding wake-flow in time averaged velocity and vorticity plots.

Performance of the flapping foil power generator is highly influenced by side-walls. Constrained flow has minor effect on non-sinusoidal flapping as compared to sinusoidal flapping. An improvement up to 6.52% in power generation efficiency is attained with optimum placement of side-walls for non-sinusoidal cases compared to free flow, $\Delta T_R = 0.4$ still has the highest efficiency

of 15.20% in constrained flow with non-dimensional side-wall distance of $d_w = 0.5$. Placing the side-walls in close proximity of $d_w = 0.1$ location results in degraded performance on mean power generation for all cases. The wall effect is particularly conspicuous for the sinusoidal case; although the instantaneous power coefficient due to pitching motion ($C_{P\theta}$) shows small increments when the flat plate sinusoidally reverse direction near the walls with close proximity, $C_{Py}$ in the translational direction is higher for $d_w = 1.0$ and 0.5 with an adverse effect when $d_w = 0.1$ where the vortex is compressed by the wall, stays attached to the upper surface for an extended period and stretches along the wall direction after shedding. The sinusoidal flapping flat plate can achieve 27.85% increase in efficiency in constrained flow with $d_w = 0.5$ compared to the free flow and 43.50% increase when $d_w = 1.0$, markedly outperforming the highest power extraction case of non-sinusoidal flapping in free flow.

The results imply that there's an optimum wall distance using side-walls in flapping foil power generation that might be a way to compensate for the loss from stroke reversals at maximum and minimum plunge positions predominantly for sinusoidal flapping.

### REFERENCES

Ashraf, M. A., A. Isaacs, J. Young, J. C. Lai and T. Ray (2009). Numerical simulation and multi-objective design of flow over oscillating airfoil for power extraction. *In Conference on modelling fluid flow (CMFF09), 14th International Conference on Fluid Flow Technologies,* Budapest, Hungary.

Ashraf, M., J. Young, J. Lai and M. Platzer (2011). Numerical analysis of an oscillating-wing wind and hydropower generator. *AIAA Journal*, 49, 1374-1386.

Davids, S. T. (1999). *A computational and experimental investigation of a flutter generator.* Doctoral dissertation. Monterey, California: Naval Postgraduate School.

Dumas, G. and T. Kinsey (2006). Eulerian simulations of oscillating airfoils in power extraction regime. *Advances in Fluid Mechanics* 245-254.

Fenercioglu, I. and O. Cetiner (2012). Categorization of flow structures around a pitching and plunging airfoil. *Journal of Fluids and Structures* 31, 92-102.

Fenercioglu, I. and O. Cetiner (2014). Effect of unequal flapping frequencies on flow

structures. *Aerospace Science and Technology* 35, 39-53.

Fenercioglu, I., B. Zaloglu, J. Young, M. A. Ashraf, J. C. S. Lai and M. F. Platzer (2015). Flow Structures Around an Oscillating-Wing Power Generator. *AIAA Journal* 53(11), 3316-3326.

Hu, H., L. Clemons and H. Igarashi (2011). An experimental study of the unsteady vortex structures in the wake of a root-fixed flapping wing. *Experiments in Fluids* 51, 347-359.

Jones, A. R., C. W. P. Ford and H. Babinsky (2011). Three-Dimensional Effects on Sliding and Waving Wings. *Journal of aircraft* 48, 633-644

Jones, K. D., C. M. Dohring and M. F. Platzer (1998). Experimental and computational investigation of the Knoller-Betz effect. *AIAA Journal* 36(7), 1240-6.

Jones, K. D. and M. F. Platzer (2010). Design and development considerations for biologically inspired flapping-wing micro air vehicles. *Animal Locomotion* 237–248.

Karakas, F. and I. Fenercioglu (2015). Effects of three-dimensionality for an oscillating-wing power-generator. *8th Ankara International Aerospace Conference* AIAC-2015-032.

Karakas, F., B. Zaloglu, I. Fenercioglu, C. Hoke, J. Young, J. Lai and M. F. Platzer (2016). On optimal oscillating-foil power generation in free and constrained flow. *In 54th AIAA Aerospace Sciences Meeting* AIAA-2016-2070.

Kaya, M. and I. Tuncer (2007). Nonsinusoidal Path Optimization of a Flapping Airfoil. *AIAA Journal* 45, 2075-2082.

Kinsey, T. and G. Dumas (2008). Parametric study of an oscillating airfoil in a power-extraction regime. *AIAA Journal* 46, 1318-1330.

Kruyt, J. W., G. F. van Heijst, D. L. Altshuler and D. Lentink (2015). Power reduction and the radial limit of stall delay in revolving wings of different aspect ratio. *Journal of the Royal Society Interface* 12(105), 20150051.

Licht, S. C., M. S. Wibawa, F. S. Hover and M. S. Triantafyllou (2010). In-line motion causes high thrust and efficiency in flapping foils that use power downstroke. *Journal of Experimental Biology* 213, 63-71.

McKinney, W. and J. DeLaurier (1981). The wingmill: an oscillating-wing wind-mill. *Journal of Energy*, 5, 109-115.

Naderi, A., M. Mojtahedpoor and A. Beiki (2016). Numerical Investigation of Non-Stationary Parameters on Effective Phenomena of a Pitching Airfoil at Low Reynolds Number. *Journal of Applied Fluid Mechanics* 9(2), 643-651.

Peng, Z. and Q. Zhu (2009). Energy harvesting through flow-induced oscillations of a foil. *Physics of Fluids* 21(12), 123602.

Platzer, M. F., M. A. Ashraf, J. Young and J. C. Lai. (2010). Extracting Power in Jet Streams: Pushing the Performance of Flapping-Wing Technology. *In 27th International Congress of the Aeronautical Sciences*, Nice, France 19-24.

Platzer, M., M. Ashraf, J. Young and J. Lai (2009). Development of a new oscillating-wing wind and hydropower generator. *In Proceedings of the 47th AIAA Aerospace Sciences Meeting* AIAA-2009-1211.

Platzer, M., N. Sarigul-Klijn, J. Young, Ashraf M., J. Lai (2014). Renewable Hydrogen Production Using Sailing Ships. *Journal of Energy Resources Technology* 136, 021203-1–5.

Rehimi, F., F. Aloui and S. B. Nasrallah (2011). Reorganization of Coherent Structures Downstream a Circular Cylinder Located between Two Parallel Walls. *Journal of Applied Fluid Mechanics* 4(2), 51-56.

Saffman, P. G. (1965). The lift on a small sphere in a slow shear flow. *Journal of Fluid Mechanics* 22, 385-400.

Shyy, W., H. Aono, S. K. Chimakurthi, P. Trizila C. Kang, C. E. S. Cesnik and H. Liu (2010). Recent progress in flapping wing aerodynamics and aeroelasticity. *Progress in Aerospace Sciences* 46, 284-327.

Son, O. and O. Cetiner (2015). Effect of Aspect Ratio and Leading and Trailing Edge Form on the Flow around an Impulsively Flat Plate. *53rd AIAA Aerospace Sciences Meeting* AIAA-2015-1296.

Son, O. and O. Cetiner (2016). Drag Prediction in the Near Wake of a Circular Cylinder Based on DPIV Data. *Journal of Applied Fluids Mechanics* 9(4) 1963-1968.

Turam, E., O. Paca, I. Fenercioglu and O. Cetiner (2015). Force measurements and estimation based on DPIV data for a plunging flat plate. *8th Ankara International Aerospace Conference* AIAC-2015-117.

Usoh, C. O., J. Young, J. C. Lai and M. A. Ashraf. (2012). Numerical analysis of a non-profiled plate for flapping wing turbines. In *Proceedings of the 18th Australasian Fluid Mechanics Conference*, Launceston, Australia.

Visbal, M., T. O. Yilmaz and D. Rockwell (2013). Three-dimensional vortex formation on a heaving low-aspect-ratio wing : Computations and experiments. *Journal of Fluids and Structures* 38, 58–76.

Westwood, A. (2004). Ocean power: Wave and tidal energy review. *Refocus* 5, 50-55.

Wu, J., Y. L. Qiu, C. Shu and N. Zhao (2014). Pitching-motion-activated flapping foil near solid walls for power extraction: A numerical investigation. *Physics of Fluids* 26(8), 083601.

Wu, J., N. Zhao (2013). Ground Effect on Flapping Wing. *Procedia Engineering* 67, 295-302.

Xiao, Q., W. Liao, S. Yang and Y. Peng (2012). How motion trajectory affects energy extraction performance of a biomimic energy generator with an oscillating foil?. *Renewable Energy* 37, 61–75.

Young, J., J. C. S. Lai and M. F. Platzer (2014). A review of progress and challenges in flapping foil power generation. *Progress in Aerospace Sciences* 67, 1-28.

Yu, M., Z. J. Wang and H. Hu (2013). Formation of Bifurcated Wakes behind Finite Span Flapping Wings. *AIAA Journal* 51, 2040-2044.

Zhu, Q. and Z. Peng (2009). Mode coupling and flow energy harvesting by a flapping foil. *Physics of Fluids* 21, 033601.